AD 668 997

ESR AND OPTICAL ABSORPTION STUDIES ON TRANSITION METAL IONS AND COLOR CENTERS IN GLASS

Elias Snitzer, et al

American Optical Company
Southbridge, Massachusetts

March 1968

RESEARCH CENTER

AMERICAN OPTICAL COMPANY

Southbridge, Massachusetts

TR 599-2

ESR AND OPTICAL ABSORPTION STUDIES OF TRANSITION METAL IONS AND COLOR CENTERS IN GLASS

SEMI ANNUAL TECHNICAL REPORT
NUMBER TWO

1 April 67 - 30 September 67

ARPA Order No. 306
Contract No. N00014-67-C-0186

Prepared by

Research Division
American Optical Company
Southbridge, Massachusetts

Project Manager - Dr. Elias Snitzer
Project Scientist - Robert J. Landry
Project Scientist - Joseph T. Fournier

March 1968

This research is part of Project DEFENDER under the joint sponsorship of the Advanced Research Projects Agency, Department of Defense and the Office of Naval Research.

ABSTRACT

A description of the work being carried out to measure the zero field splitting parameter |2D| of isolated Cr^{3+} ions in glass is given. The experimental program to measure the magnitude of the isotropic exchange coupling constant |J| for antiferromagnetically exchange coupled Cr^{3+} ion pairs in glass is described. This includes a description of an electronic integrating circuit fabricated during this period which allows direct recordings of the paramagnetic absorption. From this study it was possible to estimate that J is on the order of 60 cm^{-1}. Anistropies and lineshapes for this system are then considered. In addition, from the frequency dependence of the ESR spectrum of the exchange coupled Cr^{3+} ion pairs, a zero field splitting on the order of 0.05 cm^{-1} for the S = 1 multiplet is estimated. The optical absorption and activation spectra for ultraviolet induced permanent color center defects in a laser glass with and without Nd^{3+} is presented. Their optical absorption spectra are identical. However, the activation spectrum for the glass without the Nd^{3+} peaks at 216 nm whereas with the Nd^{3+}, the peak is shifted to 220 nm. Both activation spectra have a full width at half maximum of 13.0 nm. For the transient color centers, it is demonstrated that the presence of Nd^{3+} is not essential to the production of the transient color centers which give rise to laser self Q-switched action in glass.

A theoretical discussion of the optical and magnetic properties of a hole trapped on a SiO_4 tetrahedron with one non-bridging oxygen is presented. The hole states are described in terms of localized molecular orbitals involving the silicon ion and the non-bridging oxygen ion only. The effects of nearby alkali ions are determined in a crystal field approximation. Expressions relating the principal values of the g-tensor to electronic energies and molecular orbital expansion coefficients are obtained. The g-values are estimated for two possible molecular configurations using a semi-phenomenological approach in which electronic energy differences are tied to observed optical absorption energies. Results are compared with existing data on trapped hole centers.

CONTENTS

ILLUSTRATIONS

ESR AND OPTICAL ABSORPTION STUDIES OF TRANSITION METAL IONS AND COLOR CENTERS IN GLASS

Semi-Annual Report Number Two

1. INTRODUCTION

As in the first period, the work performed on this contract during the second semi-annual period can be classified into studies of transition metal ions in glass, experimental studies of color center defects in glass, and theoretical investigation of color center defects in glass.

The program of study of the transition metal ions in glass has been concerned with a study of the Cr^{3+} ion in glass. Experiments to measure the magnitude of the zero field splitting parameter $|2D|$ of isolated Cr^{3+} ions in glass were undertaken. A direct observation of the zero field splitting absorption has not yet been observed. Efforts to more precisely determine the frequency range for $|2D|$ are in progress and are described in the text.

Attempts to measure the magnitude of the isotropic exchange coupling constant $|J|$ for antiferromagnetically coupled Cr^{3+} ion pairs in glass were successfully undertaken and a preliminary J value was obtained. This work involved the fabrication of an electronic integrating circuit which is described in the text along with a complete description of the experimental work which allowed the estimate of the J value. In addition, the anisotropic terms which give rise to zero field splittings of the Spin multiplets for this system are considered. Experimentally, from the frequency dependence of the ESR spectrum for this system, it was possible to obtain an estimate of the zero field splitting of the $S = 1$ level.

The experimental color center defect studies in laser glass includes investigations of both permanent and transient color centers and are described in section 3.

Finally, a description of a theoretical investigation of trapped hole centers in glass is contained in section 4.

2. TRANSITION METAL IONS IN GLASS

2.1 Zero Field Splitting of Isolated Cr^{3+} Ions in Glass

The zero field splitting K-Band ESR spectrometer shown in Fig. 4 of Semi-Annual Technical Report Number One was fabricated. Experiments were subsequently undertaken to measure the distribution function in the zero-field splitting of isolated Cr^{3+} ions in a phosphate glass. In the frequency range 18-26kMHz, it has not yet been possible to directly observe absorption due to isolated Cr^{3+} ions in zero magnetic field. Either the zero-field splitting does not lie in this frequency range or the spectrometer used is not sensitive enough to allow observation of the absorption.

It may be possible to roughly determine the proper zero-field splitting range by performing additional ESR experiments in the regions of 24kMHz and 36kMHz. Theoretical analyses of an $s = 3/2$ system show that when $h\nu \gg 2D$, where $2D$ is the zero-field splitting parameter, an ESR spectrum is obtained which is predominantly centered about $g' = 2$, where $g' = h\nu/\beta H$; whereas when $h\nu \ll 2D$, an ESR spectrum centered about an higher effective g-value is obtained.[1] The spectrometer fabricated can be used as a conventional ESR spectrometer at 24kMHz, and with the addition of microwave components in the K_a-Band, ESR experiments can also be performed at 36kMHz. ESR experiments at 24kMHz and at 36kMHz are planned. After the proper frequency range has been established, experiments to directly observe zero-field splitting will be undertaken again. The question of necessary spectrometer sensitivity will be deferred until the preliminary ESR experiments to establish the proper frequency are completed.

2.2. Exchange Coupled Cr^{3+} Pairs in Glass

2.2.1 Introduction - A study of the optical and electron spin resonance spectra of a chromium doped phosphate glass as a function of chromium ion concentration has led us to infer the presence of exchange coupled Cr^{3+} pairs.[2] It has been shown that the observed ESR spectrum is consistent with a spin-Hamiltonian in which the isotropic exchange interaction dominates the Zeeman interaction which, in turn, dominates all anisotropic interactions. The pertinent spin-Hamiltonian is

$$H_s = J\,\vec{S}_1 \cdot \vec{S}_2 + g\beta\,\vec{H} \cdot (\vec{S}_1 + \vec{S}_2)\ . \qquad (1)$$

In a quantization for which S_1^2, S_2^2, S^2 and S_z $(\vec{S}=\vec{S}_1+\vec{S}_2)$ are diagonal, and with H directed along the z axis, the eigenvalues of Eq. (1) are given by

$$E = \frac{1}{2}\left[J\ S(S+1)-S_1(S_1+1)-S_2(S_2+1)\right] + g_e\ \beta\ H\ M_s \qquad (2)$$

With J positive, the resulting energy level scheme is that shown in Fig. 1.

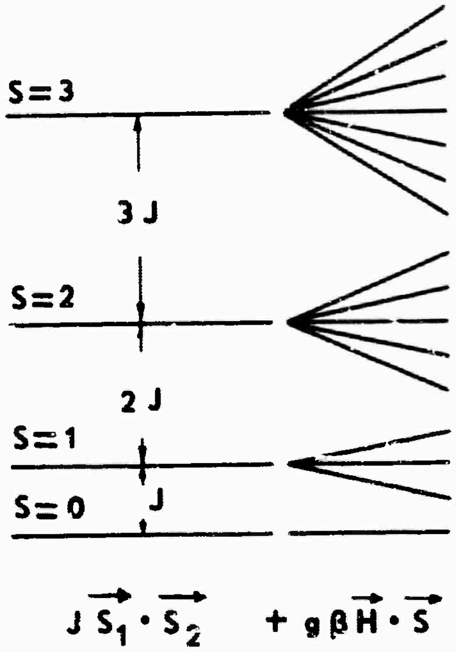

Fig. 1. Energy-level scheme for exchange coupled Cr^{3+} ion pairs. The constant J is considered to be large so that no transitions between different S levels can be induced at 9.49 kMHz.

If, as we have supposed, the separation of the S-manifolds greatly exceeds the Zeeman splitting, then the ESR transitions occur between sublevels of the S-manifolds, and all transitions have effective g-value $g_{eff} \approx g_e$. This result is consistent with observation.[2]

2.2.2 Isotropic Exchange Coupling Constant J

An estimate of the exchange coupling constant J can be obtained from the temperature dependence of the intensity of the ESR spectrum. The observed spectrum is in fact a superposition of lines due to transitions within the various S-levels. The population of the S-manifolds is temperature dependent, and consequently the contribution to the spectrum from a particular manifold varies with temperature in a well-known fashion. From the experimental view-point, it is most convenient to measure the intensity of the pairing spectrum relative to that of some standard. The ratio of the intensity $I(T)$ of the Cr^{3+} pair spectrum to the intensity $I_0(T)$ of a free electron is given by the expression

$$\frac{I(T)}{I_0(T)} \propto \frac{2e^{-J/kT} + 4e^{-3J/kT} + 6e^{-6J/kT}}{1 + 3e^{-J/kT} + 5e^{-3J/kT} + 7e^{-6J/kT}} \qquad (3)$$

A series of $I(T)/I_0(T)$ vs. kT curves for values of J in the range of 20 cm^{-1} to 500 cm^{-1} is shown in Fig. 2. The temperature range has been chosen to extend from liquid nitrogen to room temperature, and all curves have been normalized to a maximum relative intensity of 10.

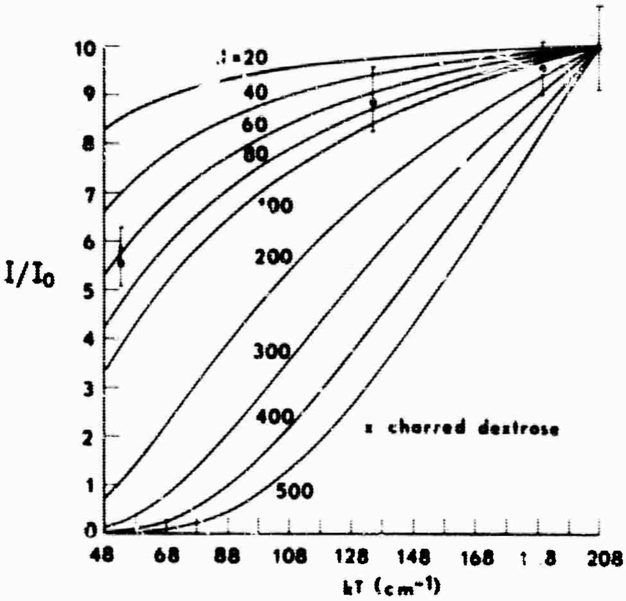

Fig. 2. Temperature dependence of the intensity of the ESR spectrum for antiferromagnetically exchange coupled Cr^{3+} pairs for values of J in the range 20 cm^{-1} to 500 cm^{-1}. The theoretical curves for the J values indicated are the solid curves. The experimental data are contained within the error bars.

The intensity of the ESR spectrum is proportional to the area under the absorption curve. When the first derivative of the ESR spectrum is obtained, a tedious and cumbersome double numerical integration must be carried out in order to obtain the area under the absorption curve. Further, small errors introduced in the first derivative curve due to baseline drift become greatly magnified when carried through the double integration procedure. Experimentally, it was found that it is extremely difficult and very time consuming to obtain an ESR spectrum of the Cr^{3+} pairs which did not contain an intolerable amount of error. The error introduced by baseline drift mentioned above is caused by a $\vec{J} \times \vec{E}$ interaction of eddy currents in the brass cavity walls due to the 100 Hz magnetic field modulation with the slowly varying DC magnetic field. The effect can be minimized by changing the angle which the DC magnetic field makes with the brass cavity walls. The adjustment required is a fine one and is almost impossible to accomplish on the broad first derivative curve of the paired Cr^{3+} ions at 9.49 kMHz shown in Fig. 3 Therefore, an integrating circuit was designed and fabricated which allows for a direct recording of the absorption. Recordings and adjustments can then be made until the baseline drift is completely eliminated from the absorption curve.

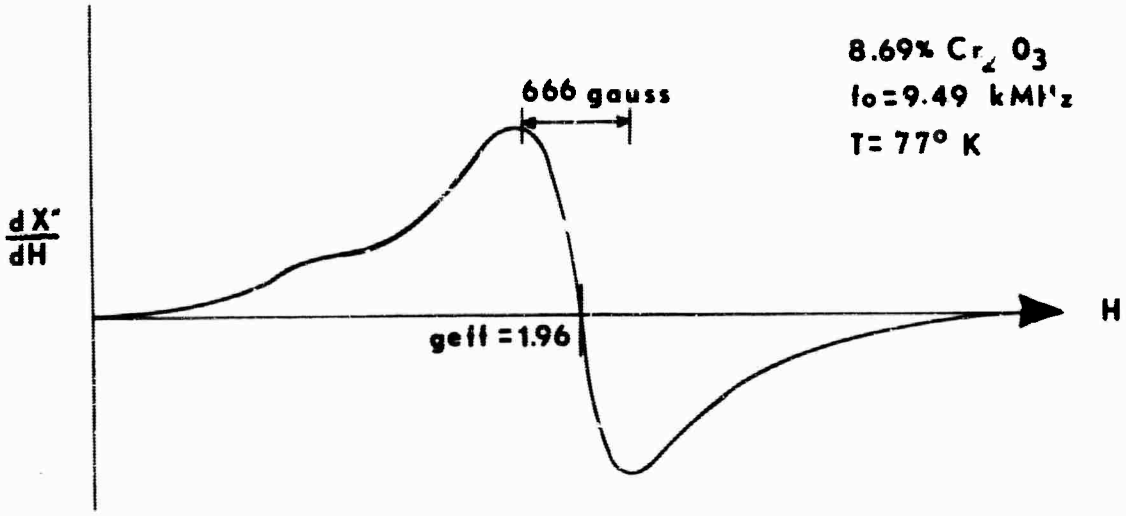

Fig. 3. ESR spectrum of phosphate glass sample which contains 8.69 wt.% Cr_2O_3 at 77° K at 9.49 kMHz showing the spectrum due to antiferromagnetically exchange coupled Cr^{3+} ion pairs.

A schematic diagram of the integrating circuit fabricated is shown in Fig. 4. The salient parts of this Miller type integrating circuit includes two operational amplifiers, a voltage dividing network, and a balancing circuit. The output of the 100 Hz amplifier phase sensitive detector is fed into a voltage divider network to obtain the appropriate input voltages to a differential input "Nexus Model SQ-10A" amplifier with available gains of 0.1x, 10x, and 1000x as determined by the 10 k-ohm resistor and the resistors in parallel with the SQ-10A amplifier. The single ended output from the SQ-10A is ther fed to a

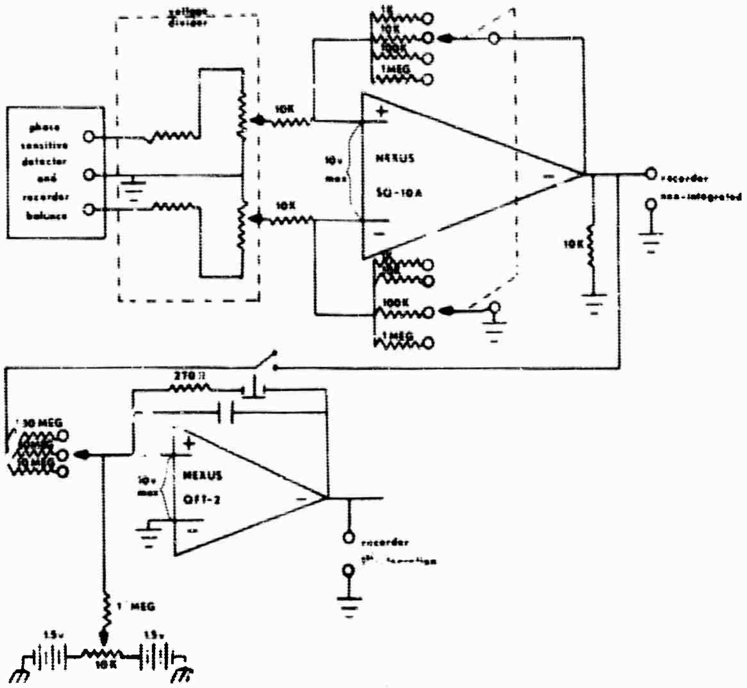

Fig. 4. Schematic diagram of integrating circuit used to obtain direct recordings of paramagnetic absorption spectra.

"Nexus QFT-2" integrating amplifier with available integrating times of 100 sec, 500 sec, and 1000 sec, as determined by the 10 μf capacitor and the input resistors. The output from the "Nexus QFT-2" is then recorded on a Varian G-14 pen recorder. The DC unbalance at the output of the "Nexus QFT-2" integrating amplifier must be less than 0.1 millivolt in order to obtain meaningful results. In addition to the balancing trimmer pots provided on the operational amplifiers, the balancing circuit shown in Fig. 4 was added at the input to the integrating amplifier in order to more easily obtain the required balance quoted above. All resistors are of 1% tolerance and in addition, only temperature compensated resistors are used in the integrating circuit. The 10 k-ohm resistor at the output of the "SQ-10A" is simply a load resistor, and this value provides for optimum performance from the amplifier. The first derivative of the absorption spectrum can be obtained at the output of the first operational amplifier, and the absorption spectrum can be obtained at the output of the second operational amplifier.

Power is supplied to the operational amplifiers from a "Newport Laboratories Model P100 (all silicon) dual DC Power Supply".

Power saturation experiments on the Cr^{3+} pair spectrum show that in the temperature region from 77° K through 323° K there are no observable power saturation effects below 1 milliwatt of microwave power incident upon a rectangular TE_{102} microwave cavity.

In this experiment, both the $S = 1/2$ standard and the chromium glass sample must be loaded into the same microwave cavity. As can be seen from Fig. 3, the ESR spectrum which arises from the exchange coupled Cr^{3+} pairs is about 4000 gauss in extent and has its absorption peak at $g' = 1.96$. Any $S = 1/2$ standard sample will have its ESR absorption superimposed on the chromium spectrum near the chromium peak and will be on the order of a few gauss wide. For this reason, it is necessary to record the absorptions of the Cr^{3+} pairs and the standard separately at two different magnetic field sweeps for a given spectrometer sensitivity. In addition, since the resonant frequency of the microwave cavity is temperature dependent, it is necessary to record the absorption of the standard sample over a constant g' value range rather than over a constant H value range. In this way, the same number of chromium spins will contribute to the area under the absorption curve for the standard sample at all temperatures. This constant error then simply changes the effective concentration of the standard sample. The standard sample used was diphenyl-picryl-hydrazil (DPPH) which has the free electron g value (2.0023) and is about 3 gauss wide at 9.49 kMHz. All experiments were performed near the microwave frequency of 9.49 kMHz with a superheterodyne ESR spectrometer with a 100 Hz modulation amplitude of 1/2 gauss.

At a given temperature, the experimental procedure consisted of recording the absorption curve due to the Cr^{3+} pairs, changing the magnetic field sweep only, and subsequently obtaining two recordings of the absorption due to the DPPH. The intensity of the standard was obtained twice at a given spectrometer. If the intensity of the standard did not reproduce to within 5% the data was not accepted since failure to reproduce to 5% is a good indication of poor klystron stabilization and hence poor spectrometer stability. The recorded absorption curves were then traced onto cardboard paper of uniform thickness, cut out, and weighed with an analytical balance. The intensity of the ESR spectrum is then proportional to the weight of the cardboard. Thus, for a given temperature and spectrometer sensitivity, the ratio of the intensities of the ESR spectra of the Cr^{3+} pairs to that of the standard is equal to the ratios of the weights of the cardboard paper upon which the spectra were traced. Five experimental points were taken in this fashion at temperatures of 77° K, 196° K, 273° K, and at 308° K.

As for the theoretical curves shown in Fig. 2, the experimental data was normalized to 10 at the room temperature water bath point. The experimental points obtained all fall within the error bars shown in Fig. 2. As a check on the above, additional experiments were performed with a different standard sample. The DPPH was replaced with charred dextrose enclosed in a vacuum tight vial and intensity measurements were performed at 77° K and at 308° K. The charred dextrose has a g-value of 1.99 and a line width of 1 gauss. The normalized check points obtained are labeled within the error bars in Fig. 2. Although there is a considerable amount of scatter in the data, the results obtained suggest a J value on the order of 60 cm^{-1}. This result should be considered as preliminary subject to additional verification.

2.2.3 Anisotropics and Lineshape - In order to assess the effect of anisotropic interactions on the ESR spectrum, it is necessary to consider a more general spin-Hamiltonian than that of Eq. (1). If anisotropic crystal field effects are expressed in terms of parameters D_c and E_c with axial and orthorhombic symmetry respectively, and terms D_e and E_e (also having axial and orthorhombic symmetry) are introduced to account for anisotropic exchange effects, the extended Hamiltonian can be written in the form[3]

$$H = J/2 \left[S(S+1)-S^1(S^1+1) -S^2(S^2+1)\right] + g\beta\vec{H}\cdot\vec{S}$$

$$+ (3\alpha_s D_e + B_s D_c) \left[(S_z)^2 - \frac{1}{3} S(S+1)\right]$$

$$+ (\alpha_s E_e + \beta_s E_c) \left[(S_x)^2 - (S_y)^2\right] , \qquad (4)$$

where

$$\alpha_s = \frac{1}{2} \left[\frac{S(S+1) + 4S^1 (S^1+1)}{(2S-1)(2S+3)}\right], \qquad (5a)$$

and

$$\beta_s = \frac{3S(S+1)-3-4S^1(S^1+1)}{(2S-1)(2S+3)} , \qquad (5b)$$

and $\vec{S}^1$ and $\vec{S}^2$ are the spin angular momentum operators for ions one and two, and $\vec{S}$ is the total spin angular momentum operator.

With $J \approx 60\ \mathrm{cm}^{-1}$, the contribution of the $S = 2$ manifold to the intensity of the ESR spectrum at 77°K is about one-tenth the contribution of the $S = 1$ level. Consequently, a good estimate of the effects of the anisotropic terms can be obtained from consideration of the $S = 1$ manifold alone. It is straightforward to diagonalize H_s within the $S = 1$ manifold for the special cases where the magnetic field $\vec{H}$ lies along the principal axes of the g-tensor.[4] From the resulting energy eigenvalues, the allowed ESR transitions can be determined. It is convenient to characterize these transitions by an effective g-value defined by the relation

$$h\nu = \Delta E = g'\,\beta H\ , \qquad (6)$$

where ν is the frequency of the microwave photon inducing the transition. For the case where the splitting ΔE is much greater than the energies associated with anisotropic effects, the effective g-values are found to be given by the expressions

$$\text{H along the z axis:}\quad g' = g_e \pm \frac{D}{\beta H_z}\ , \qquad (7a)$$

$$\text{H along the x axis:}\quad g' = g_e \pm \frac{D-3E}{2\beta H_x}\ , \qquad (7b)$$

$$\text{H along the y axis:}\quad g' = g_e \pm \frac{D+3E}{2\beta H_y}\ . \qquad (7c)$$

In Eq. (7) g_e is the free electron g-value, and D and E are those combinations of constants which appear in the second and third terms of Eq. (4),

$$D = (3\alpha_s D_e + \beta_s D_c), \qquad (8a)$$

and

$$E = (\alpha_s E_e + \beta_s E_c)\ . \qquad (8b)$$

The significant feature of these results is the symmetry of the effective g-values about the free electron value. Thus, while the anisotropic terms contribute to the width of the powder spectrum the ESR line will be symmetrical about $g = 2.0$ as long as the transition energy $h\nu$ dominates the anisotropies. The

ESR spectrum shown in Fig. 5a indicates that this condition is well satisfied at 9.49 kMHz. In Fig. 5 is shown the ESR spectra of the phosphate base glass doped with 4.31 wt.% Cr_2O_3 at 9.49 kMHz and at 2.05 kMHz at 77°K. In this sample, the Cr^{3+} ions are predominantly exchange coupled and only a small contribution to the ESR spectrum from isolated Cr^{3+} ions is evident in low field as indicated in Fig. 5a at 9.49 kMHz. The ESR spectrum of this same sample at 2.05 kMHz as shown in Fig. 5b shows a pronounced asymmetry with an overall shift to a higher effective g value. Such a result is to be expected if the transition energy is of the same order of magnitude as the energies associated with the anisotropic terms in the spin-Hamiltonian. It is estimated, therefore, that in the case of the Cr^{3+} pairs, distortion energies of the order of 0.05 cm^{-1} are involved. Now in the case of the isolated Cr^{3+} ions, the distortion D_c due to crystal field components of axial symmetry is estimated to be about 0.5 to 1.0 cm^{-1}.[2] Since each Cr^{3+} ion of a particular pair must give rise to a large axial field at the other Cr^{3+} site,

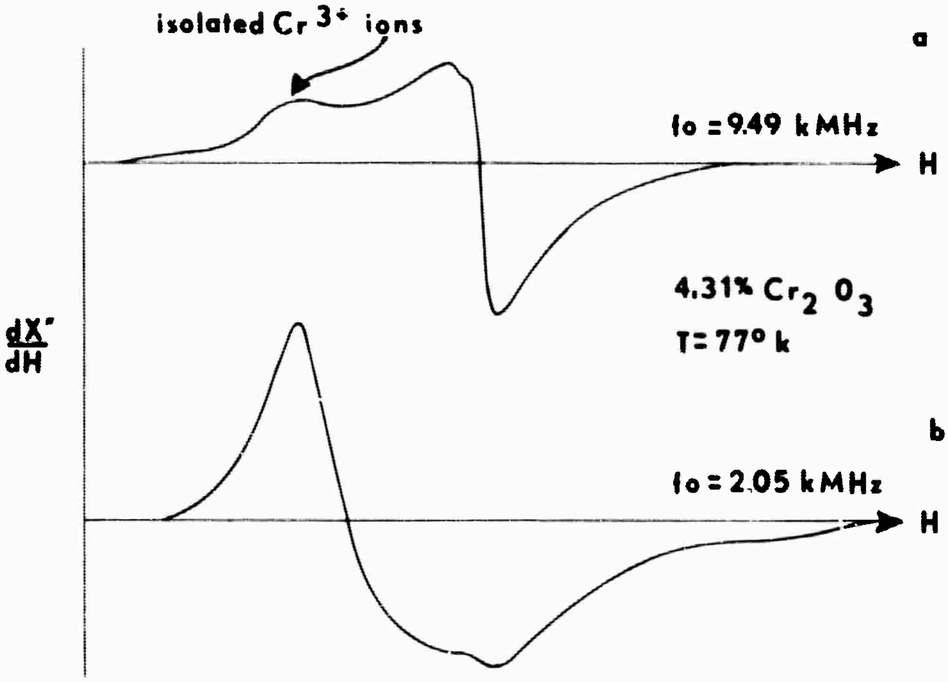

Fig. 5. Frequency dependence of ESR spectra of phosphate glass sample which contains 4.31 wt.% Cr_2O_3 at 77°K at (a) 9.49 kMHz and at (b) 2.05 kMHz at 9.49 kMHz, the ESR paramagnetic absorption peaks near $g' = 2.0$ whereas at 2.05 kMHz, the ESR paramagnetic absorption peaks at a higher effective g value.

even larger crystal field distortions are expected in the case of an ion pair. It appears then that the contribution of the exchange terms must be opposite in sign to the crystal field terms and of the order of tenths of a reciprocal centimeter.

3. EXPERIMENTAL INVESTIGATIONS OF COLOR CENTER DEFECTS IN LASER GLASS

3.1 Permanent Color Centers Defects in Glass.

In the first semi-annual report, a technique was described which allows for a fairly precise determination of the activation spectra for production of room temperature stable color centers. The optical transmission, absorption, and activation spectra for a laser base silicate glass were also shown in that report.

During this past period these experiments were repeated under more carefully controlled conditions. The activation spectrum remains as shown in the first semi-annual technical report. However, when proper account of the 'wedge' effect due to striae and non-parallelism of the flat faces is taken into account, a different optical transmission spectrum, and subsequently, a different optical absorption spectrum is obtained. The previous experiments consisted of using two flats of 2 mm thickness of the same base glass. One flat was used as a control and the second flat was solarized. The "wedge effect" between these two pieces was significant enough to completely distort the optical transmission in the regions, 300-400 nm.

In the latter experiment only one sample was used, and the optical absorption spectrum was calculated from the transmission curves before and after solarization. Although the sample still contains a significant amount of wedge, the sample is placed in the identical manner in the spectrophotometer for all transmission measurements such that the effect of wedge is minimized. This experiment was repeated on four other samples of the same base glass giving rise to the same optical absorption spectrum shown in Fig. 6. The activation spectrum for this glass is curve a in Fig. 7.

The optical absorption spectrum due to ultraviolet induced room temperature stable color centers in the same base glass above which contains in addition 5 wt.% Nd_2O_3 is identical to that shown in Fig. 6. In addition, in order to obtain the spectrum in the Nd^{3+} containing glass it is necessary to subtract the optical absorptions due to Nd^{3+}. The activation spectrum for the neodymium containing glass is shown in Fig. 7, curve b.

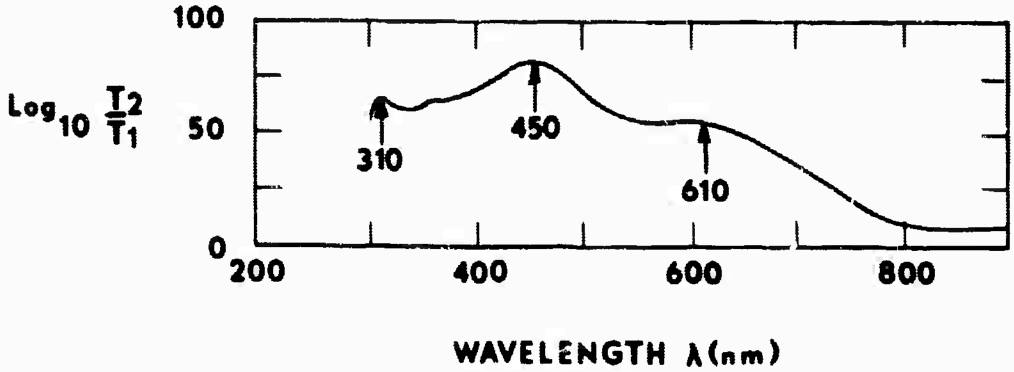

Fig. 6. Optical absorption spectrum of solarized laser glass with and without 5.0 wt.% Nd_2O_3.

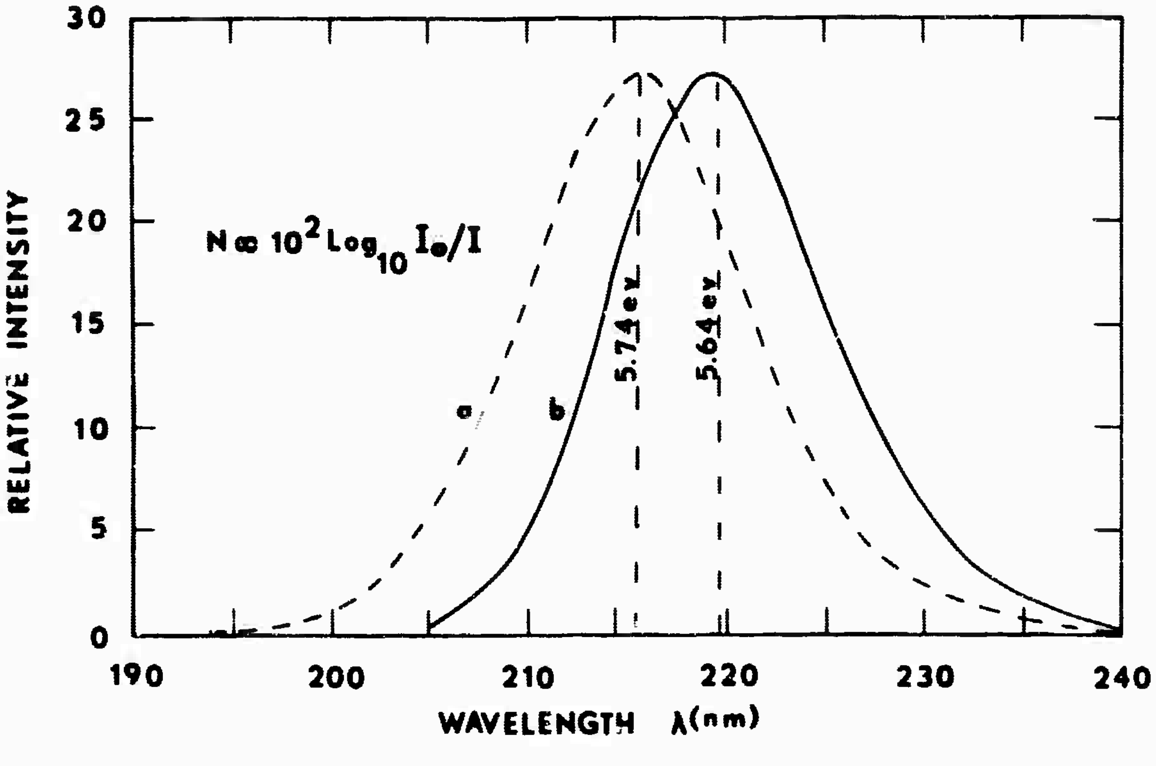

Fig. 7. Experimental activation spectra for production of permanent color center defects for 7 hours of irradiation at 300° K with a 500 watt Xenon lamp in; (a) laser base glass; and (b) laser base glass which contains in addition 5.0 wt.% Nd_2O_3.

From a comparison of curve a and b in Fig. 7, it can be seen that the effect of the addition of 5.0 wt.% Nd_2O_3 is to shift the peak of the activation spectrum to lower energy, from 5.74 ev to 5.64 ev. Thus, a smaller amount of energy is required to solarize the neodymium containing glass.

3.2 Short Lived Color Center Defects in Glass

Experiments were undertaken to determine if the presence of Nd^{3+} in the laser glass is essential to the production of the transient color centers which have an absorption at 1.06μ. A diagram of the experimental arrangement is shown in Fig. 8. The experimental laser configuration consisted of a 36.8 cm long, 2mm diameter Nd^{3+} doped laser rod with 1mm thick cladding of 'KG-12' and closed wrapped with silver foil to a 25.4 cm xenon flashtube. The clad laser rod had a polished flat on one end and a 45° roof at the other end. A 10 cm long, 2mm diameter laser Q-switching base glass without the Nd^{3+} and with parallel end flats was end coupled with water at one end to the flat end of the laser rod. The other end of the clear glass rod was coupled to a 65% dichroic at 1.06μ. Hence, end reflectances for the laser cavity of 65% and 98% were provided by the dichroic

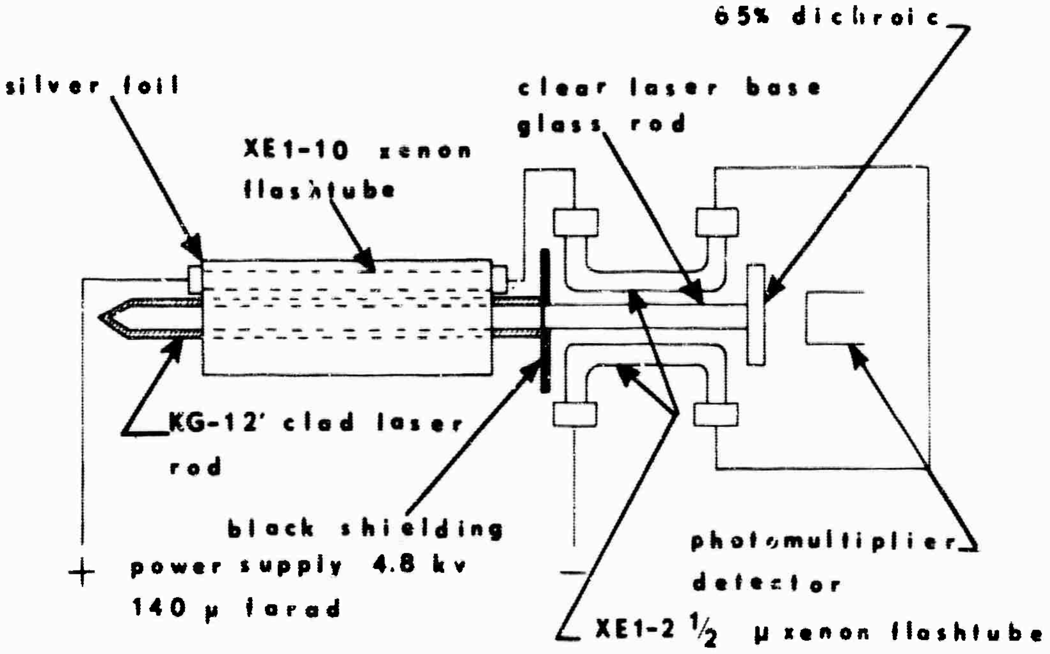

Fig. 8. Experimental laser configuration used to demonstrate that the presence of Nd^{3+} in the glass is not essential to the production of the transient laser Q-switched inducing color centers.

and the 45° roof on the laser rod, respectively. The clear glass rod was pumped with two series connected, 6.35 cm long xenon flashtubes which were connected in series with the 25.4 cm flashtube as shown in Fig. 8. The power supply was operated at 4.8 KV with a capacitance of 140μ and with an inductance of 25 mh. A total of 1620 joules was dissipated by the flashtubes, approximately 400 joules by the 6.35 cm tubes and approximately 1200 joules by the 25.4 cm flashtube. An oscilloscope trace of the laser behavior obtained when the clear glass rod is not exposed to the activating ultraviolet light is shown in Fig. 9a. The laser trace obtained when the clear glass rod is exposed to the uv is shown in Fig. 9b. In Fig. 9a it can be seen that when the ultraviolet light is filtered from the pump light with the use of soft clear glass which has strong absorptions in the uv only, normal laser damped oscillations are obtained. From this

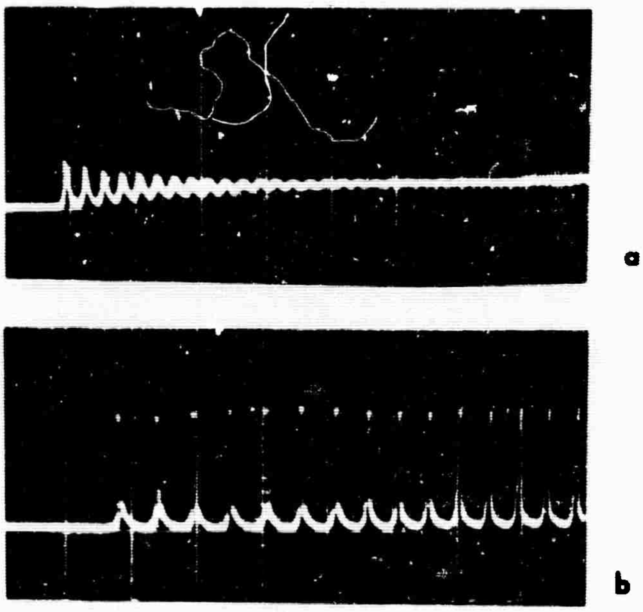

Fig. 9. Laser time traces obtained when clear glass rod is; (a) not exposed to activating ultraviolet light, and (b) exposed to activating ultraviolet light. The time traces were taken with a sweep speed of 50 sec/cm. Increasing time is from left to right.

experiment, it is possible to conclude that the presence of Nd^{3+} is not essential to the production of the transient color centers which give rise to laser self Q-switched action in glass.

4. THEORETICAL STUDIES OF TRAPPED HOLE CENTERS IN GLASS

4.1 Introduction

Among the optical absorption bands induced in uv irradiated silicate glass with composition commonly used in laser applications are two broad bands in the visible with peaks near 450 and 610 nm as shown in the first semi-annual technical report. The color centers which give rise to these bands are not unique to the laser base composition; similar absorption bands have been observed in numerous alkali and alkaline earth silicate glasses.[5,6,7] From studies of the optical absorption in binary silicate systems, it has been established that the defects are trapped holes.[6,7] Studies of the electron-spin resonance (ESR) spectrum associated with these centers suggest that the holes are trapped on SiO_4 tetrahedra with one or more non-bridging oxygen ions.[8,9,10,11]

Now both the optical absorption frequencies and the magnetic parameters determined from analysis of ESR spectra are sensitively dependent on the electronic structure of the defect center, and determination of these quantities for a particular model provides a rigorous test of that model. In addition, the optical and magnetic parameters are related in such a way that correlations can be investigated without a detailed calculation of the energy levels and wavefunctions of the defect model being considered. As previously indicated, one likely hole trapping center is the SiO_4 tetrahedron with one non-bridging oxygen ion. The research to be discussed here involves theoretical study of the electronic structure of such a tetrahedral unit undertaken to determine whether the expected optical and magnetic properties are consistent with the observed properties of the trapped hole defects. The approach is semi-phenomenological in that optical absorptions are not calculated explicitly, but are tied to observed bands. The effects of nearby alkali ions are treated in a crystal field approximation on a point ion model.

4.2 Molecular Structure of the SiO_4 Tetrahedron with One Non-Bridging Oxygen

The molecular structure of the tetrahedral SiO_4 unit with a single non-bridging oxygen can be described in the following way. Silicon 3s and 3p atomic orbitals can be combined to yield tetrahedrally directed sp^3 hybrids. These hybrid orbitals overlap strongly with oxygen hybrids and form sigma bonds.

In the case of the non-bridging oxygen, sp hybrids constructed from oxygen 2s and 2p wavefunctions are appropriate. The remaining non-hybridized oxygen 2p functions overlap Si functions and form π bonds. Focusing attention on the silicon and non-bridging oxygen only leads to the energy level scheme shown in Fig. 10.

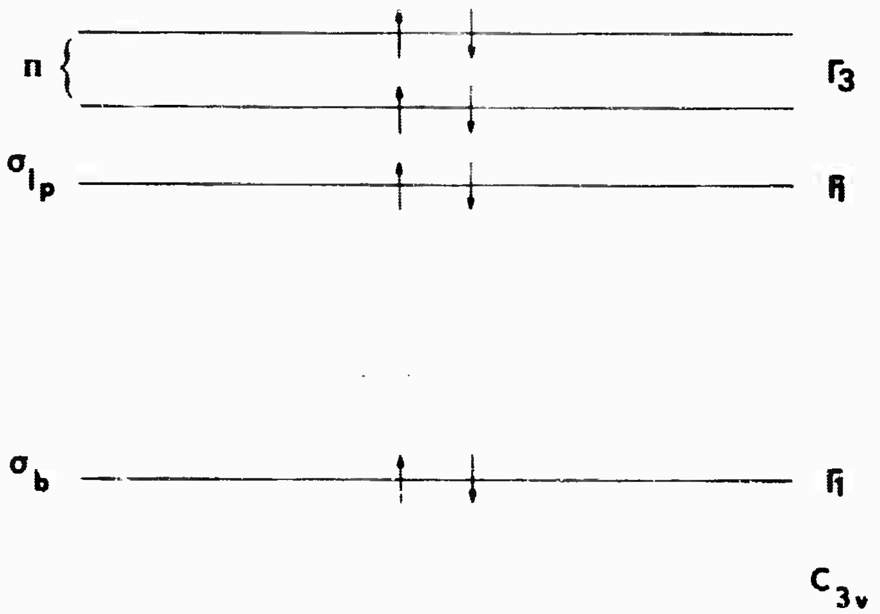

Fig. 10. Energy level diagram showing localized molecular orbitals associated with a tetrahedral SiO_4 unit with one non-bridging oxygen ion. Symmetry labels are appropriate to point group C_3v.

The lowest lying level is associated with the σ bond. The relative ordering of σ lone pair level and the π level is not known a priori, and in calculating magnetic properties both possibilities will be considered. For purpose of calculation, it is useful to describe the molecular structure in terms of localized molecular orbitals. Since the tetrahedron with one non-bridging oxygen has symmetry C_{3v}, the molecular orbitals are properly labeled by irreducible representations of this group. It can be shown that the localized σ hybrids and π functions have the proper symmetry properties and can be labeled as indicated in Fig. 10.

If the Γ_3 level lies above the $\Gamma_1(\sigma_{lp})$ level, then the hole ground state is orbitally degenerate, and a Jahn-Teller distortion would be expected. In the case of an alkali silicate glass, however, nearby alkali ions may be expected to give rise to low symmetry crystal field components which remove the degeneracy of the Γ_3 level. To take this possibility into account, we consider the effect of an alkali ion localized in one of the vertical mirror planes of tetrahedron. The symmetry is reduced to C_s, and the $\Gamma_3(C_{3v})$ level is split by the orthorhombic component of crystal field. The energy level scheme appropriate to the lower symmetry is shown in Fig. 11. Diagrams are displayed for both orderings of the sigma lone pair and π orbitals.

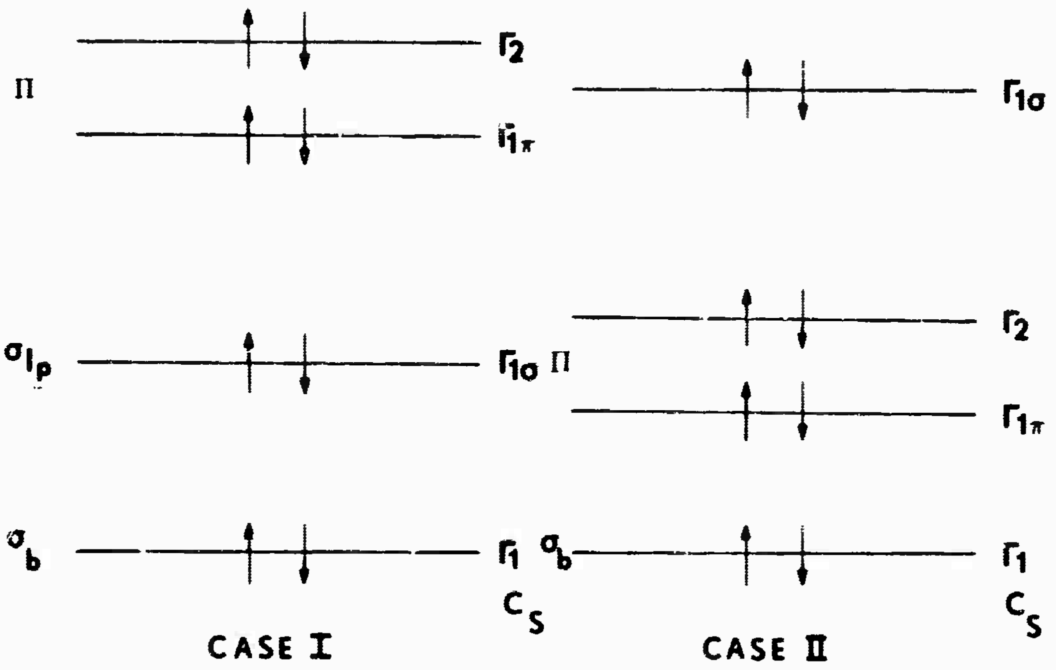

Fig. 11. Energy level diagram for a tetrahedral SiO_4 unit with one non-bridging oxygen including an orthorhombic distortion due to a nearby alkali metal ion. Symmetry labels of the localized molecular orbitals are appropriate to the point group C_s.

4.3 Magnetic Properties

In analyzing ESR spectra it is common practice to employ the so-called spin-Hamiltonian formalism. The formalism appropriate to a system with orbitally non-degenerate ground state has been developed by Pryce.[12] In his approach, the perturbation of the optical states of a system due to spin-orbit and Zeeman interactions are treated simultaneously using a projection operator technique. An effective spin-Hamiltonian involving spin operators is obtained. Application of this Hamiltonian within the ground term leads to a set of energy levels between which the spin-resonance transitions occur. For a system with spin of 1/2, the pertinent spin-Hamiltonia (neglecting nuclear hyperfine interactions) is

$$H_s = \beta\, \vec{H}\cdot\vec{g}\cdot\vec{s} \qquad (9)$$

Here, β is the Bohr magneton, $\vec{S}$ is the spin angular momentum operator, $\vec{H}$ is the applied magnetic field, and $\vec{g}$ is the g-tensor. The principal values of the g-tensor are quantities which can be determined from analysis of the ESR spectrum. It is our purpose to consider how the g-values of the trapped hole centers relate to the molecular structure of the SiO_4 tetrahedron.

The formula for the g-tensor given by Pryce is in fact appropriate to a system with a single force center only, for example, an ion in some crystal environment. The complications involved in extending the theory to systems with more than one force center have been considered by Stone[13] and by Casselman and Markham.[14] If these considerations are introduced into the theory of Pryce, one obtains the expression

$$\vec{g} = 2.0023\, \vec{1}$$

$$-\sum_n \sum_\alpha \frac{\langle 0|\sum_i \xi_\alpha(r)\vec{\ell}_i|n\rangle\langle n|\sum_j \vec{\ell}_j|0\rangle + \langle 0|\sum_j \vec{\ell}_j|n\rangle\langle n|\sum_i \xi_\alpha(r)\vec{\ell}_i|0\rangle}{E_n - E_0} \qquad (10)$$

Here, $|0\rangle$ and $|n\rangle$ denote the wavefunctions for the ground term and the n^{th} excited term respectively. The $\xi_\alpha(r)$ is given by

$$\xi_\alpha(r) = \frac{1}{r}\frac{\partial V_\alpha}{\partial r} \qquad (11)$$

where V_α is the potential associated with the α^{th} force center. The angular momentum operator $\vec{\ell}_i$ operates on coordinates of the i^{th} electron. The energies E_n are term energies.

Application of Eq. 10 to the trapped hole requires explicit expressions for the molecular wavefunctions discussed in the preceding section. These molecular orbitals expanded in terms of oxygen and silicon atomic orbitals are given by the expressions

$$\Gamma_{1\pi} = \frac{a}{2}\,(\phi_{2p\pi+} + \phi_{2p\pi-}) + \frac{b}{2}\,(\phi_{d^1} + \phi_{d^{-1}}) + \frac{c}{2}\,(\phi_{d^2} + \phi_{d^{-2}}), \tag{12a}$$

$$\Gamma^{2} = \frac{a}{2}\,(\phi_{2p\pi+} - \phi_{2p\pi-}) + \frac{b}{2}\,(\phi_{d^1} - \phi_{d^{-1}}) + \frac{c}{2}\,(\phi_{d^2} - \phi_{d^{-2}}), \tag{12b}$$

$$\Gamma_{1\sigma} = \frac{1}{2}\,(\phi_{2s} - \phi_{2pz}), \tag{12c}$$

$$\Gamma_{1\sigma b} = (\phi_{2s} + \phi_{2pz}) + f\,\chi^{Si}_{sp^3}\ . \tag{12d}$$

The functions ϕ_{2s} and ϕ_{2p} are oxygen atomic orbitals with subscripts $2p\pi+$ and $2p\pi-$ denoting p orbitals whose angular components are given by the spherical harmonics $Y_1{}^1$ and $Y_1{}^{-1}$ respectively. Silicon 3d orbitals with angular dependence $Y_2{}^m$ are designated $\phi_d{}^m$. The function $\chi^{Si}_{sp^3}$ is a silicon sp^3 lobe directed toward the non-bridging oxygen. The term wavefunctions $|0\rangle$, $|n\rangle$ are constructed as antisymmetrized products of those molecular orbitals occupied in the appropriate term. In Case I, for example, the ground term wavefunction is given ty

$$^2\Gamma_2 = \boldsymbol{\lambda}\Big[\Gamma_{1\sigma b}(1)\alpha(1)\ \Gamma_{1\sigma b}(2)\beta(2)\ \Gamma_{1\sigma}(3)\alpha(3)\ \Gamma_{1\sigma}(4)\beta(4)$$

$$\Gamma_{1\pi}(5)\alpha(5)\ \Gamma_{1\pi}(6)\beta(6)\ \Gamma_2(7)\alpha(7)\Big] \tag{13}$$

where α and β are the usual spin functions and $\boldsymbol{\lambda}$ is the antisymmetrizer. In this function the hole is located in the Γ_2 molecular orbital. Those excited terms for which the hole is located in $\Gamma_{1\pi}$, $\Gamma_{1\sigma}$, and $\Gamma_{1\sigma b}$ molecular orbitals are considered.

When Eq. 12 is evaluated using the indicated term functions. considerable simplification results. Neglecting two center integrals involving the spin-orbit coupling function $\xi(r)$, the following expressions for the principal values of the g-tensor are obtained:

Case I

$$\left\{\begin{aligned} g_x &= 2.0023 \\ g_y &= 2.0023 - \frac{\xi_O a^2}{E_{\Gamma_2} - E_{\Gamma_{1\sigma}}} - \frac{\xi_O a^2 d^2}{E_{\Gamma_2} - E_{\Gamma_{\sigma b}}} - \frac{2b^2 c^2 \xi_{Si}}{E_{\Gamma_2} - E_{\Gamma_{1\pi}}} \\ g_z &= 2.0023 - \frac{2\left[a^2 \xi_O + \xi_{Si}(b^2+2c^2)\right]\left[a^2+b^2+c^2\right]}{E_{\Gamma_2} - E_{\Gamma_{1\pi}}} \end{aligned}\right. \qquad (14)$$

Case II

$$\left\{\begin{aligned} g_z &= 2.0023 \\ g_y &= 2.0023 - \frac{a^2 \xi_O}{E_{\Gamma_{1\pi}} - E_{\Gamma_{1\sigma}}} \\ g_z &= 2.0023 - \frac{a^2 \xi_O}{E_{\Gamma_2} - E_{\Gamma_{1\sigma}}} \end{aligned}\right. \qquad (15)$$

In Eq. 14 and Eq. 15 ξ_O is the spin-orbit coupling constant for a 2p electron on the oxygen center and ξ_{Si} is the spin-orbit coupling constant for a 3d electron on the silicon center. In order to obtain an estimate of the magnitude of the g-values, we first consider the case where the electrons are localized on the oxygen center ($a \approx 1$, $b = c = 0$) and the electrons in the σ bond are equally shared ($d \approx f \approx 0.7$). The spin-orbit coupling constant ξ_O may be taken as 135 cm^{-1}, a value appropriate to O^-.[15] The energy difference ($E_{\Gamma_2} - E_{\Gamma_{1\sigma}}$) may reasonably be equated to an optical absorption energy. If, with Schreurs,[10] we associate the 450 mμ band with the center having orthorhombic symmetry, then ($E_{\Gamma_2} - E_{\Gamma_{1\sigma}}$) ≈ 20,000 cm^{-1}. The splitting ($E_{\Gamma_2} - E_{\Gamma_{\sigma b}}$) may be considered to be in the ultraviolet, ($E_{\Gamma_2} - E_{\Gamma_{1\sigma b}}$) > 50,000 cm^{-1}. The splitting ($E_{\Gamma_2} - E_{\Gamma_{1\pi}}$) due to the orthorhombic component of the crystal potential can be estimated in a point ion model. As shown in Appendix I, a reasonable value is

$(E_{\Gamma_2} - E_{\Gamma_{1\pi}}) \approx 2000\ \mathrm{cm}^{-1}$. The resulting g-values are:

Case I: $g_z = 2.0023$; $g_x = 2.009$; $g_y = 2.010$

Case II: $g_x = 2.0023$; $g_y = 2.011$, $g_z = 2.136$

4.4 Comparison with Experiment

The ESR spectrum of the trapped hole centers is complex and appears to be a superposition of two lines.[6,9,10,11] Schreurs has decomposed the spectrum into two spectra with g-values $g_\parallel = 2.013$, $g_\perp = 2.009$ (center I) and $g_1 = 2.003$, $g_2 = 2.009$, $g_3 = 2.019$ (center II).[11] Now the extremely high value of g_z obtained in Case II ($g_z = 2.136$) is certainly inconsistent with observation; no portion of the hole spectrum extends to such high g-values. Furthermore, since the calculated g-shift is about an order of magnitude larger than the largest observed g-shift, it is unlikely that use of the actual values of the molecular orbital expansion parameters or a refined value of $(E_{\Gamma_2} - E_{\Gamma_{1\pi}})$ could bring the calculated g-shifts within the range of observed values. Consequently, the structure considered in Case II seems to be ruled out as a source of the hole-like absorption.

In Case I, however, the calculated g-values are within the range of the observed values. With this ordering of the energy levels, the g-values are relatively insensitive to the orthorhombic distortion. Since the g-values cannot be measured with accuracy greater than about 0.001, the difference in g_x and g_z could not be resolved, and this defect would appear to have axial symmetry. However, comparison of these calculated g-values ($g_\parallel = 2.010$, $g_\perp = 2.0023$) with the g-values resulting from Schreurs' decomposition ($g_\parallel = 2.013$, $g_\perp = 2.009$) shows that the results are incompatible. A further inconsistency arises from Schreurs' observation that the spectrum due to the axial defect predominates in samples of high alkali metal concentration,[10] while tetrahedra with a single non-bridging oxygen ion should predominate for low alkali metal concentration. Since the components of the trapped hole spectrum overlap strongly, other possible decompositions cannot be ruled out. Nevertheless, it is not possible on the basis of our results to establish the SiO_4 tetrahedron with one non-bridging oxygen as a source of the trapped hole absorptions. Schreurs has suggested tetrahedra with two and three non-bridging oxygen ions as the respective sources of the orthorhombic and axial components of the trapped hole spectrum.[10] It would be of interest to consider these models. However, these structures are somewhat more complex, and correlations between optical and magnetic properties may be more difficult to analyze.

APPENDIX I

We wish to calculate the first order splitting of the $\Gamma^3(C_{3v})$ level due to the orthorhombic component of crystal field due to a single alkali ion located in one of the vertical mirror planes of the tetrahedron. If $V(\vec{r})$ is the crystal potential due to the alkali ion, then the energy splitting ΔE is given by

$$\Delta E = \langle \Gamma_2 | -eV(\vec{r}) | \Gamma_2 \rangle - \langle \Gamma_{1\pi} | -eV(r) | \Gamma_{1\pi} \rangle , \qquad \text{(A-1)}$$

where Γ_2 and $\Gamma_{1\pi}$ are the molecular orbitals given in Eq. 4. The potential $V(\vec{r})$ is determined from the expression

$$V(r) = \sum_{\ell=0}^{\infty} \sum_{m=0}^{\ell} r^{\ell} P_{\ell}^{m}(\cos\theta) \left[c_{\ell m} \cos\phi + d_{\ell m} \sin\phi \right] , \qquad \text{(A-2)}$$

where

$$c_{\ell m} = \sum_{\alpha} \frac{q_a}{r_\alpha^{\ell+1}} (2 - \delta_{m0}) \frac{(\ell - m)!}{(\ell + m)!} P_{\ell}^{m}(\cos\theta_\alpha) \cos m\phi_\alpha , \qquad \text{(A-3a)}$$

and

$$d_{\ell m} = \sum_{\alpha} \frac{q_A}{r_\alpha^{\ell+1}} (2 - \delta_{m0}) \frac{(\ell - m)!}{(\ell + m)!} P_{\ell}^{m}(\cos\theta_\alpha) \sin m\phi_\alpha . \qquad \text{(A-3b)}$$

These equations provide an expression for the crystal potential at field point $\vec{r}$ due to point ions with charge q_α located at $\vec{r}_\alpha$.

In evaluating Eq. A1, a number of simplifications can be introduced. From symmetry requirements, all terms involving constants $d_{\ell m}$ vanish. If only single-center terms are retained in evaluating matrix elements, then since at most silicon 3d functions are involved, the series for $V(r)$ truncates at $\ell = 4$. In fact, the only constants required are c_{22}^{O}, c_{22}^{Si}, c_{42}^{Si}, and c_{44}^{Si}. Because the $c_{\ell m}$ fall off as $r_\alpha^{\ell+1}$, c_{22} is expected to be the dominant factor in determining the splitting of the levels.

The resulting expression for ΔE is given by

$$\Delta E = N_{22}\; c(1,2,1;-1,2,1) \left[a^2 \quad c_{22}^{O} \; \langle r^2 \rangle_{2p}^{O} \quad \langle 1||2||1\rangle \right.$$
$$\left. + \; b^2 \; c_{22}^{Si} \; \langle r^2 \rangle_{3d}^{Si} \quad \langle 2||2||2\rangle \right] \; . \qquad \text{(A-4)}$$

Here, N_{22} is a normalization constant, $c(1,2,1;-1,2,1)$ is a Clebsch-Gordon coefficient and the matrix elements $\langle 1||2||1\rangle$ and $\langle 2||2||2\rangle$ involve spherical harmonics only. The parameters a and b are the molecular orbital expansion coefficients, c_{22}^{O} and c_{22}^{Si} are crystal constants at the oxygen and silicon sites respectively, and $\langle r^2 \rangle_{2p}^{O}$ and $\langle r^2 \rangle_{3d}^{Si}$ are the expectation values of r^2 for an oxygen 2p and a silicon 3d orbital respectively. In keeping with our previous assumption, we take $a \approx 1$, $b \approx 0$ in first approximation.

Determination of c_{22}^{O} due to a single positive alkali metal ion in a vertical reflection plane is straightforward. An appropriate coordinate system is shown in Fig. A1.

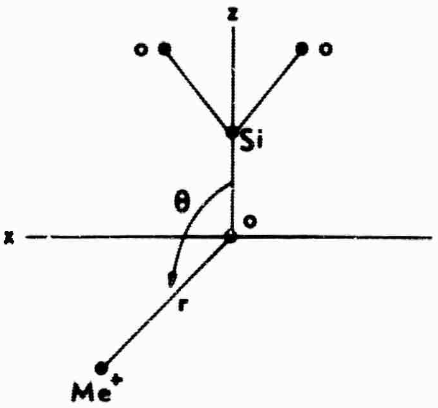

Fig. A1. Coordinate scheme for evaluation of the constant ε_{22}^{0} due to a single positive alkali metal ion located in a vertical reflection plane of the SiO_4 tetrahedron.

If r is the distance from the non-bridging oxygen to the alkali metal ion, and θ locates the metal ion in the vertical reflection plane, then c_{22}^{O} is given by

$$c_{22}^{O} = \frac{1}{4r^3} \; \sin^2 \theta \; . \qquad \text{(A-5)}$$

Taking $\langle r^2 \rangle^{O}_{2p} = 1\ 98$ a.u.[15] and substituting in Eq. (A-4) leads to a maximum splitting of 2000 cm^{-1}. The positive value of ΔE indicates that the $\Gamma_{2\pi}$ level is elevated while the $\Gamma_{1\pi}$ level is dperessed, as shown in Fig. 11.

REFERENCES

1. L. L. van Reijan, "Electron Spin Resonance Studies of Pentavalent and Trivalent Chromium," (Doctoral Thesis) Technological University at Einclhoven, 1964).

2. R. J. Landry, J. T. Fournier and C. G. Young, J. Chem. Phys. 46, 1285 (1967).

3. J. Owen, J.A.P., Supplement to Vol. 32, 213 (1961).

4. C. J. Ballhausen, "Introduction to Ligand Field Theory" (McGraw-Hill Book Co., Inc. New York, 1962), pp. 138-139.

5. A. Kats and J. M. Stevels, Philips Res. Rept. 11, 115 (1956).

6. J. S. Stroud, J. Chem. Phys. 35, 844 (1961).

7. J. S. Stroud, J. Chem. Phys. 37, 836 (1962).

8. G. O. Karapetyan and D. M. Yudin, Soviet Phys.-Solid State 4, 1943, (1963).

9. J. W. H. Schreurs and R. F. Tucker, in Proceedings of the International Conference on the Physics of Non-Crystalline Solids, Delft, 1964, J. A. Prins, Editor (North-Holland Publ. Co., Amsterdam, 1964), p. 616.

10. J. W. H. Schreurs, J. Chem. Phys. 47, 818 (1967).

11. T. A. Sidorov and V. A. Tiulken, Akademia Nauk S.S.S.R. Doklady 175, 872 (1967)

12. M. H. L. Pryce, Proc. Phys. Soc. (London) A63, 25 (1950).

13. A. J. Stone, Proc. Roy. Soc. (London) A271, 424 (1963).

14. T. N. Casselman and J. J. Markham, J. Chem. Phys. 42, 4178 (1965).

15. R. H. Bartram, C. E. Swenberg, and J. T. Fournier, Phys. Rev. 139, A941 (1965).

Unclassified

Security Classification

DOCUMENT CONTROL DATA - R&D

(Security classification of title, body of abstract and indexing annotation must be entered when the overall report is classified)

1. ORIGINATING ACTIVITY *(Corporate author)*

Research Division
American Optical Corporation
Southbridge, Massachusetts 01550

2a. REPORT SECURITY CLASSIFICATION
Unclassified

2b. GROUP
N/A

3. REPORT TITLE

ESR and Optical Absorption Studies of Transition Metal Ions and Color Centers in Glass.

4. DESCRIPTIVE NOTES *(Type of report and inclusive dates)*

Semi Annual Report No. 2, 1 April 67 - 30 September 1967

5. AUTHOR(S) *(Last name, first name, initial)*

Landry, Robert J.
Fournier, Joseph T.

6. REPORT DATE	**7a. TOTAL NO. OF PAGES**	**7b. NO. OF REFS**
March 1968	25 + iii	15

8a. CONTRACT OR GRANT NO.
N00014-67-C-0186

b. PROJECT NO.
ARPA ORDER 306

c.

d.

9a. ORIGINATOR'S REPORT NUMBER(S)

TR-599-2

9b. OTHER REPORT NO(S) *(Any other numbers that may be assigned this report)*

10. AVAILABILITY/LIMITATION NOTICES

Qualified requestors may obtain copies of this report from DDC. Distribution of this document is ulimited.

11. SUPPLEMENTARY NOTES

Research is part of Project DEFENDER

12. SPONSORING MILITARY ACTIVITY

Office of Naval Research
Department of the Navy
Washington, D.C.

13. ABSTRACT

A description of the work being carried out to measure the zero field splitting parameter |2D| of isolated Cr^{3+} ions in glass is given. The experimental program to measure the magnitude of the isotropic exchange coupling constant |J| for antiferromagnetically exchange coupled Cr^{3+} ion pairs in glass is described. This includes a description of an electronic integrating circuit fabricated during this period which allows direct recordings of the paramagnetic absorption. From this study, it was possible to estimate that J is on the order of 60 cm^{-1}. Anistropies and lineshapes for this system are then considered. In addition, from the frequency dependence of the ESR spectrum of the exchange coupled Cr^{3+} ion pairs, a zero field splitting on the order of 0.05 cm^{-1} for the $S = 1$ multiplet is estimated. The optical absorption and activation spectra for ultraviolet induced permanent color center defects in a laser glass with and without Nd^{3+} is presented. Their optical absorption spectra are identical. However, the activation spectrum for the glass without the Nd^{3+} peaks at 216 nm whereas with the Nd^{3+}, the peak is shifted to 220 nm. Both activation spectra have a full width at half maximum of 13.0 nm. For the transient color centers, it is demonstrated that the presence of Nd^{3+} is not essential to the production of the transient color centers which give rise to laser self Q-switched action in glass.

A theoretical discussion of the optical and magnetic properties of a hole trapped on a SiO_4 tetrahedron with one non-bridging oxygen is presented. The hole states are described in terms of localized molecular orbitals involving the silicon ion and the non-bridging oxygen ion only. The effects of nearby alkali ions are determined in a crystal field approximation. Expressions relating the principal values of the g-tensor to electronic energies and molecular orbital expansion coefficients are obtained. The g-values are estimated for two possible molecular configurations using a semi-phenomenological approach in which electronic energy differences are tied to observed optical absorption energies. Results are compared with existing data on trapped hole centers.

DD FORM 1 JAN 64 1473

Unclassified

Security Classification

14. KEY WORDS	LINK A		LINK B		LINK C	
	ROLE	WT	ROLE	WT	ROLE	WT
Glass						
Glass Structure						
Laser Glass						
Lasers						
ESR Measurements						
Color Centers						

INSTRUCTIONS

1. **ORIGINATING ACTIVITY:** Enter the name and address of the contractor, subcontractor, grantee, Department of Defense activity or other organization (*corporate author*) issuing the report.

2*a*. **REPORT SECURITY CLASSIFICATION:** Enter the overall security classification of the report. Indicate whether "Restricted Data" is included. Marking is to be in accordance with appropriate security regulations.

2*b*. **GROUP:** Automatic downgrading is specified in DoD Directive 5200.10 and Armed Forces Industrial Manual. Enter the group number. Also, when applicable, show that optional markings have been used for Group 3 and Group 4 as authorized.

3. **REPORT TITLE:** Enter the complete report title in all capital letters. Titles in all cases should be unclassified. If a meaningful title cannot be selected without classification, show title classification in all capitals in parenthesis immediately following the title.

4. **DESCRIPTIVE NOTES:** If appropriate, enter the type of report, e.g., interim, progress, summary, annual, or final. Give the inclusive dates when a specific reporting period is covered.

5. **AUTHOR(S):** Enter the name(s) of author(s) as shown on or in the report. Enter last name, first name, middle initial. If military, show rank and branch of service. The name of the principal author is an absolute minimum requirement.

6. **REPORT DATE:** Enter the date of the report as day, month, year; or month, year. If more than one date appears on the report, use date of publication.

7*a*. **TOTAL NUMBER OF PAGES:** The total page count should follow normal pagination procedures, i.e., enter the number of pages containing information.

7*b*. **NUMBER OF REFERENCES:** Enter the total number of references cited in the report.

8*a*. **CONTRACT OR GRANT NUMBER:** If appropriate, enter the applicable number of the contract or grant under which the report was written.

8*b*, 8*c*, & 8*d*. **PROJECT NUMBER:** Enter the appropriate military department identification, such as project number, subproject number, system numbers, task number, etc.

9*a*. **ORIGINATOR'S REPORT NUMBER(S):** Enter the official report number by which the document will be identified and controlled by the originating activity. This number must be unique to this report.

9*b*. **OTHER REPORT NUMBER(S):** If the report has been assigned any other report numbers (*either by the originator or by the sponsor*), also enter this number(s).

10. **AVAILABILITY/LIMITATION NOTICES:** Enter any limitations on further dissemination of the report, other than those imposed by security classification, using standard statements such as:

(1) "Qualified requesters may obtain copies of this report from DDC."

(2) "Foreign announcement and dissemination of this report by DDC is not authorized."

(3) "U. S. Government agencies may obtain copies of this report directly from DDC. Other qualified DDC users shall request through
____."

(4) "U. S. military agencies may obtain copies of this report directly from DDC. Other qualified users shall request through
____."

(5) "All distribution of this report is controlled. Qualified DDC users shall request through
____."

If the report has been furnished to the Office of Technical Services, Department of Commerce, for sale to the public, indicate this fact and enter the price, if known.

11. **SUPPLEMENTARY NOTES:** Use for additional explanatory notes.

12. **SPONSORING MILITARY ACTIVITY:** Enter the name of the departmental project office or laboratory sponsoring (*paying for*) the research and development. Include address.

13. **ABSTRACT:** Enter an abstract giving a brief and factual summary of the document indicative of the report, even though it may also appear elsewhere in the body of the technical report. If additional space is required, a continuation sheet shall be attached.

It is highly desirable that the abstract of classified reports be unclassified. Each paragraph of the abstract shall end with an indication of the military security classification of the information in the paragraph, represented as *(TS)*, *(S)*, *(C)*, or *(U)*.

There is no limitation on the length of the abstract. However, the suggested length is from 150 to 225 words.

14. **KEY WORDS:** Key words are technically meaningful terms or short phrases that characterize a report and may be used as index entries for cataloging the report. Key words must be selected so that no security classification is required. Identifiers, such as equipment model designation, trade name, military project code name, geographic location, may be used as key words but will be followed by an indication of technical context. The assignment of links, roles, and weights is optional.